IEEE Photonics Journal
An IEEE Photonics Society Publication

Open Access

Nonperpendicular Incidence Induced Spatial Frequency Drift in Polarized Low-Coherence Interferometry and Its Compensation

Volume 7, Number 6, December 2015

Tiegen Liu
Junfeng Shi
Junfeng Jiang
Kun Liu
Shuang Wang
Jinde Yin
Shengliang Zou

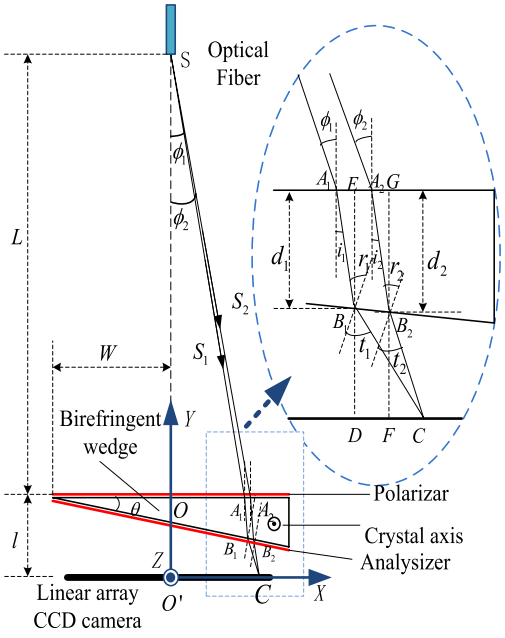

DOI: 10.1109/JPHOT.2015.2494505
1943-0655 © 2015 IEEE

IEEE photonics SOCIETY

IEEE

Nonperpendicular Incidence Induced Spatial Frequency Drift in Polarized Low-Coherence Interferometry and Its Compensation

Tiegen Liu,[1,2] Junfeng Shi,[1,2] Junfeng Jiang,[1,2] Kun Liu,[1,2] Shuang Wang,[1,2] Jinde Yin,[1,2] and Shengliang Zou[1,2]

[1]College of Precision Instrument and Opto-Electronics Engineering, Tianjin University, Tianjin 300072, China
[2]Key Laboratory of Opto-Electronics Information Technical, Tianjin University, Ministry of Education, Tianjin 300072, China

DOI: 10.1109/JPHOT.2015.2494505

Manuscript received September 1, 2015; revised October 20, 2015; accepted October 20, 2015. Date of publication October 26, 2015; date of current version November 25, 2015. This work was supported in part by the National Instrumentation Program of China under Grant 2013YQ030915; by the National Basic Research Program of China under Grant 2010CB327802; by the National Natural Science Foundation of China under Grant 61227011, Grant 61378043, Grant 61475114, and Grant 11004150; by Tianjin Natural Science Foundation under Grant 13JCYBJC16200; by the Science and Technology Key Project of the Chinese Ministry of Education under Grant 313038; and by Shenzhen Science and Technology Research Project under Grant JCYJ20120831153904083. Corresponding author: J. Jiang (e-mail: jiangjfjxu@tju.edu.cn).

Abstract: We establish an optical path difference (OPD) distribution model in a spatial scanned polarized low-coherence interferometry (LCI) considering the nonperpendicular incidence of light to explore the spatial frequency drift. Simulation shows that the OPD is no longer linearly distributed on a charged coupled device (CCD) and that the spatial frequency drifts approximately linearly as low coherent interference fringe (LCIF) shifts. A compensation process for spatial frequency domain analysis (SFDA)-based algorithm is proposed to avoid interference-order misidentification and consequent jump error. We verified our analysis and effectiveness of the proposed algorithm with an optical fiber Fabry–Pérot pressure sensing experiment. The measured spatial frequency drift agreed well with simulation results, and the interference-order misidentification was eliminated.

Index Terms: Sensors, fiber optics system, novel methods.

1. Introduction

Low-coherence interferometry (LCI) is an important method for 3-D profiling [1]–[3] and optical coherence tomography [4] and has been introduced into optical fiber sensing to measure parameters that can be transferred to absolute length or distance, such as pressure, temperature, displacement, and so forth [5]–[7].

Two main kinds of demodulation algorithms, fringe-pattern-based algorithms and phase-based algorithms, are developed for LCI. Fringe-pattern-based algorithms utilize peak position of interference envelope [8], [9] or central fringe peak position [10] to acquire shift information of the

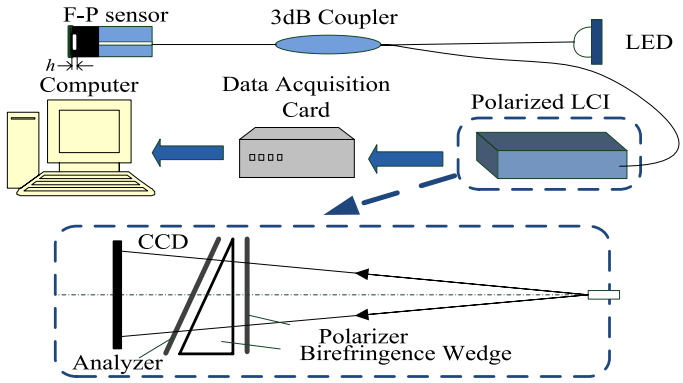

Fig. 1. Schematic layout of optical fiber F–P pressure sensing system based on polarized LCI.

interferogram. It has the advantages of simplicity and fast speed. However, the measurement is vulnerable to interferogram distortion [11] resulting from non-vertical incidence of light, random noise of detector and light source variation in polarized LCI [12]. Phase-based algorithms, such as spatial frequency domain analysis (SFDA) based algorithms, extract absolute phase [5] or phase slope information [13] of interference fringe to realize demodulation. The high sensitivity nature of the phase makes high precision demodulation available. Since phase slope requires a good linearity of phase, which may not be fulfilled, absolute phase can achieve better demodulation result, but this kind of algorithm often encounters with the problem of interference-order misidentification [14] because of non-ideal system parameters and causes jump errors in calculated absolute phases [15]. Non-vertical incidence light is a typical non-ideal system parameter and gives rise to spatial frequency drift problem in SFDA-based algorithm, which means central spatial frequency cannot keep constant in the whole measurement range and will deteriorate the demodulation precision. There is little discussion on that in previous literature.

In this paper, we established the optical path difference (OPD) distribution mathematical model for a spatial scanned polarized LCI considering the non-perpendicular incidence light to explore the spatial frequency drift. Then we analyzed the influence of spatial frequency drift in SFDA-based algorithm and proposed a compensation algorithm to circumvent interference-order misidentification problem. The analysis and proposed algorithm were verified in an optical fiber Fabry–Pérot pressure sensing system. The measured spatial frequency drift agreed well with simulation results, and the problem of jump error was eliminated successfully.

2. Analysis of Non-Vertical Incidence of Light and Its Induced Spatial Frequency Drift

The polarized LCI configuration is shown schematically in Fig. 1, which is a modified version of the system demonstrated by Dändliker in 1992 [16]. Light from LED broadband source is coupled into an 2×2 optical fiber coupler and launched into an F–P sensor. The sensor is fabricated by a silicon slice bonded on a glass base with a small groove on it. This structure constitutes a small F–P cavity whose length equals the depth of the small groove. The light is then modulated and reflected by the F–P cavity, the cavity length of which is proportional to air pressure. Since the reflectivity of both the two reflectors is small, reflected light can be approximately considered as two-beam-interference. The reflected light then projects into polarized LCI demodulation module, which is consisted of a polarizer, a birefringent wedge and an analyzer. The polarization directions of polarizer and analyzer are vertical to each other, and 45° angle to optical axis of the wedge. When the light goes into the birefringent wedge, it is divided into extraordinary (E) light and ordinary (O) light, introducing an optical path difference (OPD) after analyzer. When the OPD caused by the thickness of wedge equals that of the cavity length of F–P sensor, the low coherent interference fringe (LCIF) appears and is received by a linear array charged coupled device (CCD) camera.

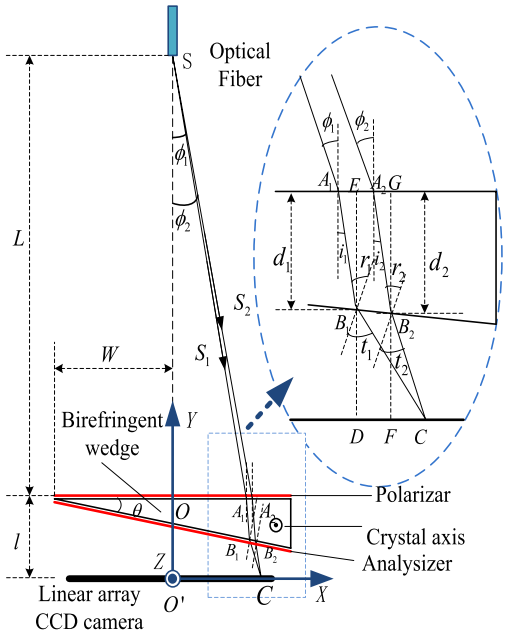

Fig. 2. Practical configuration of polarized LCI and beam propagation paths with non-perpendicular incidence of light.

Considering the Gaussian spectrum of light source, the LCIF signal can be expressed as

$$I(\Delta l, h) = \exp\left\{-\left[\frac{(\Delta l - 2h)\Delta k}{4\sqrt{\ln 2}}\right]^2\right\}\cos[(\Delta l - 2h)k_0] \tag{1}$$

where $k_0 = 2\pi/\lambda_0$ is the central wave number of the light source, λ_0 is the central wavelength, $\Delta k = 2\pi\Delta\lambda/\lambda_0^2$, $\Delta\lambda$ is the source 3 dB spectral width, h is the cavity length of the sensor, and Δl is the OPD caused by the birefringent wedge. The ideal OPD is uniformly distributed and can be simply expressed as $\Delta l = \Delta n \cdot d$, where Δn is the refractive index difference between O-light and E-light, d is the thickness of the birefringent wedge and has a linear relationship with the CCD pixel number, which can be used to denote the interferogram position. The LCIF appears at the position where $d = 2h/\Delta n$, which shifts linearly with the cavity length h.

Fringe-pattern-based algorithms and SFDA-based algorithms achieve demodulation by detecting the peak position or the phase of the interferogram along with the CCD pixel array. Thus, linear distribution of OPD is expected, and it requires that incident light is parallel, perpendicular to the birefringent wedge surface and CCD should be in contact with the hypotenuse of wedge in order to neglect the refraction effect on both sides of the wedge. For convenience of practical module layout and compactness, we use divergent beam instead of collimated beam as shown in Fig. 2. To make a more compact demodulation module, we can put a small negative lens behind optical fiber to diverge beams further, and therefore, the light can cover the whole CCD range with a shorter distance. This will lead to the non-linear distribution of OPD. Thus, the non-perpendicular incidence of light must be taken into consideration.

Fig. 2 shows the beam propagation paths for polarized LCI considering the non-perpendicular incidence of light. Since O-light shows different refractive index with E-light, non-perpendicular incidence of light will make the geometric optical paths of O-light and E-light, which reach the same point of the CCD, do not superpose each other. In the figure, the O-light and E-light rays are designated by S_1 and S_2, respectively. The OPD of S_1 and S_2 can be written as

$$\Delta l = (\overline{SA_1} + n_o\overline{A_1B_1} + \overline{B_1C}) - (\overline{SA_2} + n_e\overline{A_2B_2} + \overline{B_2C}) \tag{2}$$

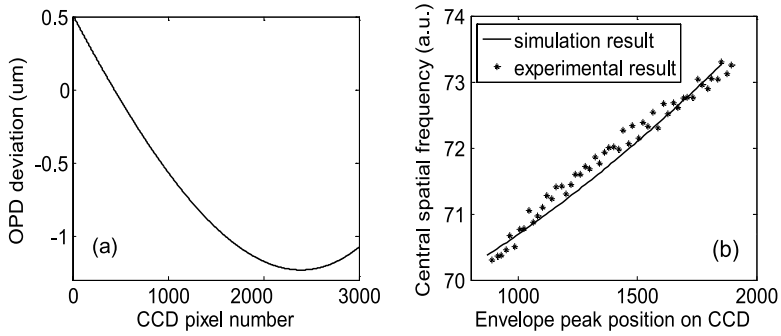

Fig. 3. (a) OPD deviation distribution (OPD distribution deviation is calculated by subtracting the ideal OPD $\Delta n \cdot d$ from Δl). (b) Central spatial frequency comparison between simulation result and experimental result.

where $\overline{SA_1}$, $\overline{A_1B_1}$, $\overline{B_1C}$, $\overline{SA_2}$, $\overline{A_2B_2}$, and $\overline{B_2C}$ are the geometric lengths; and n_o, n_e are the refraction indexes of O-light and E-light in the wedge, respectively. As shown in Fig. 2, we establish a rectangular coordinate system and define the midpoint of linear array CCD camera as the origin. ϕ_1 and ϕ_2 are the incidence angles of S_1 and S_2, respectively. i_1, i_2, t_1 and t_2 represent the refraction angles at point A_1, A_2, B_1 and B_2, respectively. d_1 and d_2 represent the thickness of the wedge at point B_1 and B_2, respectively. L is the distance from the optical fiber to the front surface of the wedge, θ is the wedge angle and l is the distance from CCD to the front surface of the wedge.

The OPD corresponding to each pixel of CCD can be expressed as

$$\Delta l(\phi_1, \phi_2) = \left[\frac{L}{\cos\phi_1} + n_o\frac{d_1}{\cos i_1} + \frac{l - d_1}{\cos(t_1 - \theta)}\right] - \left[\frac{L}{\cos\phi_2} + n_e\frac{d_2}{\cos i_2} + \frac{l - d_2}{\cos(t_2 - \theta)}\right] \tag{3}$$

where $i_1 = \arcsin(\sin\phi_1/n_o)$, $i_2 = \arcsin(\sin\phi_2/n_e)$, $t_1 = \arcsin[n_o\sin(i_1 + \theta)]$, and $t_2 = \arcsin[n_e\sin(i_2 + \theta)]$. d_1 and d_2 can be expressed by

$$d_1(\phi_1) = \frac{(L\tan\phi_1 + W)\tan\theta}{1 - \tan\theta\tan i_1}, d_2(\phi_2) = \frac{(L\tan\phi_2 + W)\tan\theta}{1 - \tan\theta\tan i_2} \tag{4}$$

where W is the half width of the wedge. From (3) and (4), we can calculate the detailed OPD distribution projected on CCD if we can establish the relationship between the CCD pixel number and the incidence angles of ϕ_1 and ϕ_2. Suppose N is the CCD pixel number corresponding to the point of C, which is the coincident point of O-light and E-light. For a CCD with 3000 pixels and 7 μm pixel width, which is used in our experimental system, the N can be expressed by ϕ_1 and ϕ_2 as

$$\begin{aligned}(N - 1500)\cdot 7\ \mu\text{m} &= \overline{OA_1} + \overline{A_1E} + \overline{DC} \\ &= L\tan\phi_1 + d_1\tan i_1 + (l - d_1)\tan(t_1 - \theta) \\ (N - 1500)\cdot 7\mu\text{m} &= \overline{OA_2} + \overline{A_2G} + \overline{FC} \\ &= L\tan\phi_2 + d_2\tan i_2 + (l - d_2)\tan(t_2 - \theta).\end{aligned} \tag{5}$$

By combining (3)–(5), we can obtain the OPD distribution on CCD with pixel number as variable. We carried out simulation to investigate the effect of the non-perpendicular incidence. The parameters $W = 15$ mm, $L = 85$ mm, $n_o = 1.3777$, $n_e = 1.3895$, $l = 7$ mm, $k_0 = 0.0105$ rad/nm, $\Delta k = 0.0030$ rad/nm, $\Delta k = 0.0030$ rad/nm, and $\theta = 0.175$ rad. Fig. 3(a) shows the distribution of OPD deviation from ideal OPD. It can be seen that the OPD distribution is no longer linear proportional to the CCD pixel number, and LCIF period will change at different positions of CCD; thus, spatial frequency will drift.

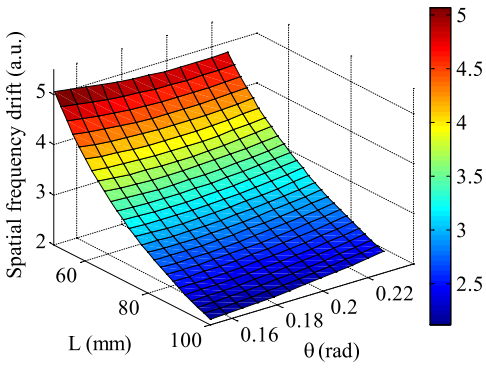

Fig. 4. Dependence of spatial frequency drift on wedge angle θ and distance L (cavity length ranging from 11.0 μm to 18.0 μm).

Fig. 3(b) shows the simulation result for h ranging from 11.0 μm to 18.0 μm. For each h corresponding to a cavity length, we use (1) to get LCIF signal by substituting a serial of ΔI. Then we detect its envelope peak position and obtain the amplitude-frequency data by fast Fourier transform (FFT). The discrete spatial frequency is represented by the serial number. The exact central spatial frequency is obtained by conducting Gaussian fitting to amplitude-frequency data. From the simulation result we can see that the central spatial frequency drifts and has an approximately linear relationship with the envelope peak position of LCIF.

In order to experimentally verify the analysis about spatial frequency drift, we conducted an experiment by placing F–P sensor in a pressure chamber. The pressure varies from 10 kPa to 260 kPa at intervals of 5 kPa, with pressure control accuracy 0.02 kPa. 20 consecutive interference signals were acquired under each pressure. The amplitude-frequency curves were obtained by conducting FFT and central spatial frequency was recorded, the relationship between central spatial frequency and envelope peak position is also shown in Fig. 3(b). The experimental result showed that the central spatial frequency drifted in the range from 70.5 to 73.5 and the central spatial frequency has an approximately linear relationship with the envelope peak position of LCIF, which agreed well with the simulation analysis.

The wedge angle θ and the distance L are two main influential factors of spatial frequency drift. Their effects on spatial frequency drift are shown in Fig. 4. Large L and small θ are preferred to alleviate the influence of spatial frequency drift. However, L may be physically limited by dimension and optical power, and θ is also limited by CCD dimension. Therefore, software compensation must be taken into account in the demodulation process.

3. Compensation of the Spatial Frequency Drift on SFDA-Based Algorithm

SFDA-based algorithm by recovering absolute phase uses intercept of phase unwrapping curve to identify interference-order and then recover the absolute phase of a selected monochromatic frequency f_0 [5]. Since spatial frequency drifts, the whole phase unwrapping curve moves. The central spatial frequency f is the function of envelope peak position X, which can be expressed by $f = f(X)$. Therefore, when calculating the intercept of the curve to recover fringe interference-order and absolute phase, an additional phase difference $\Delta\varphi(X) = -\Delta f(X) \cdot a(X)$ will exist, where $a(X)$ is the slope of phase unwrapping curve, $\Delta f(X)$ is the spatial frequency drift from f_0, which can be calculated by $\Delta f(X) = f(X) - f_0$. The phase difference introduces an error, $\Delta\varphi(X) - floor[\Delta\varphi(X)/2\pi] \cdot 2\pi$, to the calculated absolute phase, where the function $floor()$ return the integer smaller or equal to the parameter in the bracket. Since both phase slope and spatial frequency drift are linearly proportional to cavity length, this error results in a quadratic deviation from the linearity of absolute phase. When additional phase difference $\Delta\varphi(X)$ caused by spatial frequency drift is greater than 2π, interference-order identification will cause jump errors of recovered absolute phase and lead to the failure of demodulation.

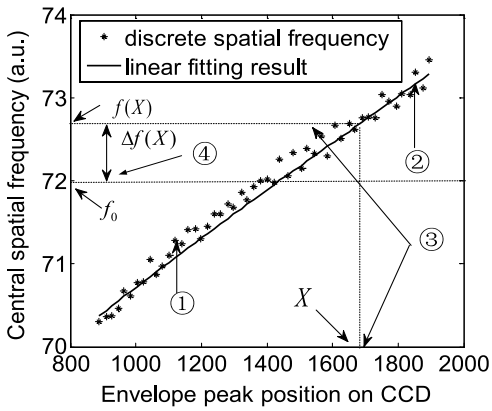

Fig. 5. Discrete central spatial frequency of different pressure and its linear fitting function; by detecting the envelope peak position X of LCIF, the exact central spatial frequency $f(X)$ can be calculated.

To compensate the phase difference $\Delta\varphi(X)$, we should obtain the exact central spatial frequency $f(X)$ of LCIFs. We get amplitude-frequency characteristic curve of the LCIF by FFT and then use Gaussian function fitting process to retrieve the central spatial frequency. However, the obtained central spatial frequency is vulnerable to random noise and can be severely deteriorated.

According to our simulation result that central spatial frequency drifts approximately linearly with envelope peak position. Our compensation algorithm can be performed by five steps, in which step ① to ④ are shown in Fig. 5 with the experimental data as an example. ①: Obtain the envelope peak positions of LCIFs, Gaussian fit the amplitude-frequency characteristic curve shapes, and get their corresponding discrete central spatial frequency by obtaining the center of the fitting Gaussian function; ②: establish the relationship between the discrete central spatial frequency and envelope peak position by linear fitting; ③: calculate the exact central spatial frequency $f(X)$ with the linear function obtained in step ② by envelope peak position X; ④: select the monochromatic frequency f_0, since the phase slope is vulnerable to random noise; the monochromatic frequency f_0 is selected the integer near the mid-value of the central spatial frequency range obtained in step ① to reduce its impact to compensation; then, calculate the spatial frequency drift value $\Delta f(X) = f(X) - f_0$; ⑤: obtain the slope $a(X)$ and intercept $\varphi(X)$ of phase unwrapping curve, calculate the phase difference by $\Delta\varphi(X) = -\Delta f(X) \cdot a(X)$, and then obtain the compensated intercept $\Delta\Phi(X)$ by subtracting the phase difference $\Delta\varphi(X)$ from the intercept $\varphi(X)$; the compensated intercept $\Delta\Phi(X)$ is then used to identify interference-order and recover the absolute phase.

In order to experimentally verify the effectiveness of our proposed algorithm, we used the same measured data in Section 2. The monochromatic frequency f_0 was selected Ω_{72} (spatial frequency corresponding to the serial number 72). Processes of SFDA-based algorithm without compensation and our proposed algorithm were conducted for demodulation. The demodulation results are showed in Fig. 6. The results showed that, the absolute phase demodulated by algorithm without compensation suffered jump error because of the interference-order misidentification, as the analysis of spatial frequency drift, while the problem was effectively solved by our proposed compensation algorithm.

4. Conclusion

In conclusion, we established the OPD distribution mathematical model of spatial scanned polarized LCI considering the non-perpendicular incidence of light to explore spatial frequency drift. Simulation shows the OPD is no longer linearly distributed on CCD and that the spatial frequency drifts approximately linearly as low-coherence interference fringe shifts. Combining the SFDA-based algorithm by recovering the absolute phase, we analyzed the influence of spatial frequency

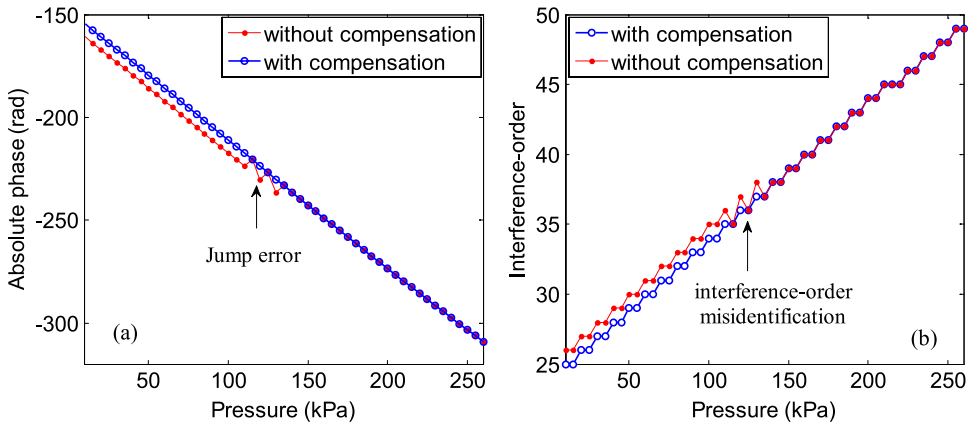

Fig. 6. Absolute phase–pressure curves (a) and interference-order (b) comparison of the proposed compensation algorithm and SFDA-based algorithm without compensation.

drift and proposed a compensation algorithm to eliminate its caused interference-order misidentification. Our analysis and algorithm were demonstrated in an optical fiber Fabry–Pérot pressure sensing system, and misidentification of interference-order was effectively avoided.

References

[1] K. G. Larkin, "Efficient nonlinear algorithm for envelope detection in white-light interferometry," *J. Opt. Soc. Amer. A*, vol. 13, no. 4, pp. 832–843, 1996.
[2] T. Dresel, G. Häusler, and H. Venzke, "Three-dimensional sensing of rough surfaces by coherence radar," *Appl. Opt.*, vol. 31, no. 7, pp. 919–925, Mar. 1992.
[3] P. Sandoz, R. Devillers, and A. Plata, "Unambiguous profilometry by fringe-order identification in white-light phase-shifting interferometry," *J. Mod. Opt.*, vol. 44, no. 3, pp. 519–534, 1997.
[4] L. Vabre, A. Dubois, and A. C. Boccara, "Thermal-light full-field optical coherence tomography," *Opt. Lett.*, vol. 27, no. 7, pp. 530–532, 2002.
[5] J. Jiang *et al.,* "A polarized low-coherence interferometry demodulation algorithm by recovering the absolute phase of a selected monochromatic frequency," *Opt. Exp.*, vol. 20, no. 16, pp. 18117–18126, Jul. 2012.
[6] J. G. Kim, "Absolute temperature measurement using white light interferometry," *J. Opt. Soc. Korea*, vol. 4, no. 2, pp. 89–93, 2000.
[7] L. M. Smith and C. C. Dobson, "Absolute displacement measurements using modulation of the spectrum of white light in a Michel interferometry," *Appl. Opt.*, vol. 28, no. 16, pp. 3339–3342, 1989.
[8] S. S. C. Chim and G. S. Kino, "Three-dimensional image realization in interference microscope," *Appl. Opt.*, vol. 31, no. 14, pp. 2550–2553, 1992.
[9] P. Sandoz, "Wavelet transform as a processing tool in white-light interferometry," *Opt. Lett.*, vol. 22, no. 14, pp. 1065–1067, Jul. 1997.
[10] S. Chen, A. W. Palmer, K. T. V. Grattan, and B. T. Meggitt, "Digital signal-processing techniques electronically scanned optical-fiber white-light interferometry," *Appl. Opt.*, vol. 31, no. 28, pp. 6003–6010, 1992.
[11] S. Wang *et al.,* "Zero-fringe demodulation method based on location-dependent birefringence dispersion in polarized low-coherence interferometry," *Opt. Lett.*, vol. 37, no. 2, pp. 1827–1830, 2014.
[12] W. K. Chong, X. Li, and S. Wijesoma, "Effects of phosphor-based LEDs on vertical scanning interferometry," *Opt. Lett.*, vol. 35, no. 17, pp. 2946–2948, Sep. 2010.
[13] P. de Groot and L. Deck, "Surface profiling by analysis of white-light interferograms in the spatial frequency domain," *J. Mod. Opt.*, vol. 42, no. 2, pp. 389–401, 1995.
[14] Y. S. Ghim and A. Davies, "Complete fringe order determination in scanning white-light interferometry using a Fourier-based technique," *Appl. Opt.*, vol. 51, no. 12, pp. 1922–1928, Apr. 2012.
[15] P. de Groot, X. Colonna de Lega X, J. Kramer, and M. Turzhitsky, "Determination of fringe order in white-light interference microscopy," *Appl. Opt.*, vol. 41, no. 22, pp. 4571–4578, Aug. 2002.
[16] R. Dändliker, E. Zimmermann, and G. Frosio, "Electronically scanned white-light interferometry: A novel noise-resistant signal processing," *Opt. Lett.*, vol. 17, no. 9, pp. 679–681, May 1992.